

Two-dimensional total absorption spectroscopy with conditional generative adversarial networks

C. Dembski^{a,b,c}, M.P. Kuchera^{d,f}, S. Liddick^{b,e}, R. Ramanujan^f, A. Spyrou^{a,b,c}

^a*Department of Physics and Astronomy, Michigan State University, East Lansing, MI, 48824, USA*

^b*National Superconducting Cyclotron Laboratory, Michigan State University, East Lansing, MI, 48824, USA*

^c*Joint Institute for Nuclear Astrophysics, Michigan State University, East Lansing, MI, 48824, USA*

^d*Department of Physics, Davidson College, Davidson, NC, 28035, USA*

^e*Department of Chemistry, Michigan State University, East Lansing, MI, 48824, USA*

^f*Department of Mathematics and Computer Science, Davidson College, Davidson, NC, 28035, USA*

Abstract

We explore the use of machine learning techniques to remove the response of large volume γ -ray detectors from experimental spectra. Segmented γ -ray total absorption spectrometers (TAS) allow for the simultaneous measurement of individual γ -ray energy (E_γ) and total excitation energy (E_x). Analysis of TAS detector data is complicated by the fact that the E_x and E_γ quantities are correlated, and therefore, techniques that simply unfold using E_x and E_γ response functions independently are not as accurate. In this work, we investigate the use of conditional generative adversarial networks (cGANs) to simultaneously unfold E_x and E_γ data in TAS detectors. Specifically, we employ a Pix2Pix cGAN, a generative modeling technique based on recent advances in deep learning, to treat (E_x, E_γ) matrix unfolding as an image-to-image translation problem. We present results for simulated and experimental matrices of single- γ and double- γ decay cascades. Our model demonstrates characterization capabilities within detector resolution limits for upwards of 90% of simulated test cases.

Keywords: total absorption spectroscopy, unfolding, machine learning, neural networks, conditional generative adversarial networks

1. Introduction

Peak finding is a primary step in many forms of spectroscopic analysis and is used in a number of domains such as molecular identification [1, 2], the study of distant, high-redshift galaxies [3, 4], and in applications across nuclear sciences [5]. Peak finding is a problem well-suited to automated analysis methods and the ability of modern deep learning networks to efficiently analyze one-dimensional spectra has been shown in γ -spectroscopy [6, 7, 8] as well as in similar applications like NMR spectroscopy [9]. However, these artificial peak-isolation techniques have yet to be applied to two-dimensional spectroscopy data, an important extension necessary to account for correlations between simultaneously measured parameters. An example of such correlated parameters appears in the technique of γ -ray total absorption spectroscopy (TAS) [10, 11]. TAS measurements can provide both the individual γ -ray energy (E_γ) and total excitation energy (E_x), two parameters that are not independent from each other.

Total absorption spectroscopy is a technique used to measure all γ transitions associated with the de-excitation of excited states in a nucleus populated in β -decay. The detection of entire decay cascades, as opposed to only individual γ -rays as in traditional high-resolution spectroscopy, makes total absorption spectroscopy methods significantly less susceptible to error resulting from the Pandemonium effect [12] and makes them particularly well-suited for the measurement of β -intensity distributions [10, 11]. Multiple TAS detectors are active in current low-energy nuclear physics research, including the Decay Total Absorption Spectrometer (DTAS) detector [13], Modular Total Absorption Spectrometer (MTAS) detector [14], and Summing NaI(Tl) (SuN) detector [15]. Total absorption spectroscopy is being used to study β -strength distributions for applications in nuclear structure [16, 17, 18], reactor decay heat [19, 20, 21], and nuclear parameters relevant to astrophysical applications via techniques like the β -Oslo method [22, 23, 24, 25]. TAS detectors have also been used to measure capture reaction cross sections for astrophysical calculations [26, 27]. This work is based on measurements and simulations using the SuN detector at Michigan State University [15]. SuN is a NaI detector, 16 inches in height and 16 inches in diameter, with a 1.8 inch wide bore hole along its central axis. Additionally, SuN is segmented into eight optically isolated segments, which provide a measure of the individual γ rays participating in a cascade, while summing the total energy deposited in the detector is sensitive to the excitation energy.

A common method of consolidating the multivariate data collected by TAS detectors is to treat the γ energy and nuclear excitation energy spectra as x - and y -axis projections, respectively, of a two-dimensional (E_x, E_γ) matrix. Between the two axes, these matrices contain crucial information about the entirety of a nucleus's level scheme and are indispensable to total absorption spectroscopy.

For example, Fig. 1 shows such a 2D matrix that was created from the measurement of a ^{60}Co radioactive source placed at the center of the SuN detector. The 2D matrix has the excitation energy on the y -axis and the individual segment energy on the x -axis. The projections of the two axes are also presented in the figure. ^{60}Co decays predominantly into a level of ^{60}Ni located at 2505 keV excitation energy, which is visible in the y -axis projection of Fig. 1. This level de-excites via the emission of two sequential γ rays with energies of 1173 and 1332 keV, which are visible in the x -axis projection.

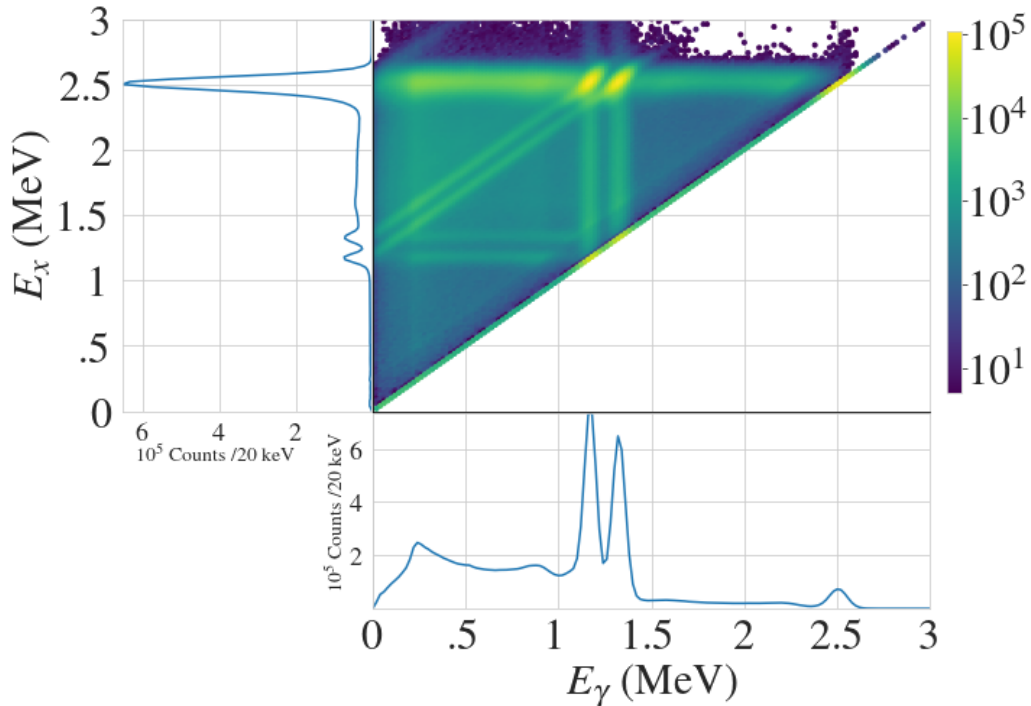


Figure 1: An (E_x, E_γ) matrix for the decay of ^{60}Co with x and y axis 1D projections, as measured by SuN.

Close examination of the (E_x, E_γ) matrix reveals the major difficulty

posed by total absorption spectroscopy. Both the excitation energy and γ energy measurements are correlated quantities. As such, unfolding the measured spectra with the detector response has to take these correlations into account. An ideal unfolding method would translate an (E_x, E_γ) matrix to a corresponding (E'_x, E'_γ) matrix that contains counts at locations corresponding to level scheme decays.

Methods such as those described in [28] have proven successful in the past, but are uniaxial and only partially eliminate correlational effects in the (E_x, E_γ) matrices. Automated unfolding has been of interest for quite some time — early attempts at machine learning-based analysis methods for one-dimensional γ -ray spectra data date back almost thirty years [29] — and recent advances in deep learning have realized the feasibility of this style of approach [30, 31, 6, 32, 33, 34]. In the present work we present a method of unfolding two-dimensional (E_x, E_γ) matrices via a conditional Generative Adversarial Network (cGAN). cGANs have been applied to a breadth of image translation and reconstruction problems in physics and biomedical imaging [35, 36, 37, 38, 39] which indicate applications to open problems in γ -ray spectroscopy.

2. Machine Learning Methods

2.1. Unfolding (E_x, E_γ) Matrices As Image-to-Image Translation

Suppose we are given a training set of ordered pairs $\mathcal{T} = \{(i, i') : i \in I \text{ and } i' \in I'\}$, where I and I' are sets of images from two domains. As a concrete example, one could consider pairs (i, i') where the samples i are drawn from daytime urban scenes, while the samples i' are the same scenes after dark. The image-to-image translation problem seeks to fit a parameterized function $f : I \mapsto I'$ that converts an instance $i \in I$ into an instance $i' \in I'$ — in our example, f would take a daytime scene and transform it into a nighttime one. Isola et al.’s landmark publication [40] was one of the earliest works to demonstrate the capacity of deep neural networks to learn such functions f from data. We cast the problem of unfolding (E_x, E_γ) matrices as an instance of image-to-image translation. Specifically, we create a dataset comprising pairs (i, i') where each i is a raw (E_x, E_γ) matrix and i' is its corresponding unfolded matrix (E'_x, E'_γ) , which serves as the training set for our image-to-image translation model.

2.2. Conditional GANs

We train a conditional Generative Adversarial Network (cGAN) to solve our image-to-image translation problem. A cGAN typically comprises two neural networks engaged in an adversarial game: a *generator* and a *discriminator*. The generator’s task is to create outputs that look realistic (i.e., that look like they may have been sampled from the target distribution), while the discriminator attempts to tell apart these “fake” samples from real ones drawn from the training data. Formally, the generator is a neural network $G : I \times Z \mapsto I'$ which models the conditional distribution $\Pr(i' | i)$, where $i \in I$ is a raw matrix (E_x, E_γ) and $i' \in I'$ is an unfolded matrix (E'_x, E'_γ) . The additional input $\mathbf{z} \in Z$ to G implements a trick that is widely used to endow neural networks with stochastic behavior: $\mathbf{z} = [z_0, z_1, \dots, z_n]$ is a noise vector whose components z_i are independently sampled from a standard distribution like $\mathcal{N}(0, 1)$. By computing $G(i, \mathbf{z})$ for a fixed i and different values of \mathbf{z} , one can obtain multiple samples from $\Pr(i' | i)$. The discriminator is a separate neural network $D : I' \mapsto [0, 1]$. Given an unfolded matrix $i' \in I'$, D outputs a score indicating the network’s belief in whether i' came from the training data or was generated by G . Higher values correspond to increased confidence that the input was a “real” sample drawn from the training set.

2.3. The Pix2Pix Architecture

We now describe Pix2Pix [40, 41], the cGAN architecture that we use in this work. Our discriminator D is inspired by the PatchGAN architecture first described by Isola et al. [40]. The key innovation in PatchGAN is to offer feedback to the generator at a more localized scale, by scoring *patches* — smaller regions of the input matrix — rather than the entire input. Further, the neural network operates on a pair of matrices (i, i') as input, so that the patch scores evaluate the quality of the translation in different parts of the matrices. Concretely, $D : I \times I' \mapsto [0, 1]^{p \times p}$, where p is the patch resolution. We fit the parameters of the discriminator by minimizing the following loss function

$$\mathcal{L}_D(D, G, \mathcal{T}) = -\frac{1}{n} \sum_{(i, i') \in \mathcal{T}} \sum_{\pi \in P} \log(D_\pi(i, i')) + \log(1 - D_\pi(i, G(i))) \quad (1)$$

where n is the number of examples in our training set \mathcal{T} , P denotes the set of all patches and D_π is the score assigned by the discriminator to patch π .

We base our generator G on the UNet autoencoder to match the network’s output dimensionality to that of the input [42]. UNet has been shown to be both computationally efficient and effective at image translation problems [42] and was also used in the original Pix2Pix system [40]. Our generator deviates from the traditional cGAN formulation in one key way: since our mapping problem is completely deterministic (i.e., there is exactly one unfolded matrix i' that corresponds to an input matrix i), we eliminate the noise vector \mathbf{z} as an input to the generator, so that G simply maps elements of I to elements of I' .

We fit the parameters of the generator by minimizing a loss function \mathcal{L}_G given by

$$\mathcal{L}_G(D, G, \mathcal{T}) = \mathcal{L}_{adv}(D, G, \mathcal{T}) + \lambda \cdot \mathcal{L}_{L1}(G, \mathcal{T}) \quad (2)$$

where

$$\mathcal{L}_{adv}(D, G, \mathcal{T}) = -\frac{1}{n} \sum_{(i,i') \in \mathcal{T}} \sum_{\pi \in P} \log(D_\pi(i, G(i))) \quad (3)$$

and

$$\mathcal{L}_{L1}(G, \mathcal{T}) = \frac{1}{n} \sum_{(i,i') \in \mathcal{T}} |i' - G(i)|. \quad (4)$$

The generator loss \mathcal{L}_G comprises two components: an adversarial term (\mathcal{L}_{adv}) and an L1-norm term (\mathcal{L}_{L1}). Minimizing the former corresponds to the generator’s samples “fooling” the discriminator into believing that they are genuine unfolded matrices drawn from the training data. Minimizing the latter ensures that the outputs of the generator are objectively close to the ground truth unfolded matrices in the dataset, under a traditional distance metric. We also considered other candidates, such as the L_2 -norm, in this second term, but we found that the L_1 loss consistently outperformed the others. Finally, the variable λ in Equation 2 is a hyperparameter that controls the relative weighting of the two loss terms. The best value for this variable was experimentally determined and is reported in Table 1, alongside the values of other key hyperparameters. We use the Adam [43] algorithm for training both the discriminator and the generator. Adam is a member of the stochastic gradient descent family that utilizes parameter-specific learning rates based on the magnitude of recently calculated gradients. It is a standard choice for training deep learning models due to its stability and speed of convergence under a wide range of conditions [44].

Epochs of training	125
Batch size	16
Generator learning rate	2×10^{-6}
Discriminator learning rate	2×10^{-6}
Generator β_1	0.5
Generator β_2	0.999
Discriminator β_1	0.5
Discriminator β_2	0.999
Generator ϵ	1×10^{-7}
Discriminator ϵ	1×10^{-7}
L_1 loss scaling factor λ	300
Patch resolution p	62

Table 1: The values of the hyperparameters used in our final model. The exponential decay rate for the first moment in the Adam optimizer is given by β_1 , while β_2 is the exponential decay rate of the second moment. The term ϵ is a constant used to ensure numerical stability in Adam.

3. Data Preparation

3.1. Data Simulation and Processing

We used the GEANT4 [45] simulation package to simulate our training data. Each training spectrum contains a decay comprising either a single γ -ray or two γ -rays emitted in sequence, mimicking simple isotopic decay cascades. We choose a binning of 500 across a 0-10 MeV range along both axes. This binning is comparable to the resolution of the SuN detector. [22, 24, 23, 25].

We simulated A total of 9950 single γ -ray decay spectra for each integer energy within the 50-10000 keV range. We further produced an additional 9451 training spectra containing cascades of two γ -rays with randomly-generated energies, for a total of 19401 training examples. The corresponding target spectra were generated as 500×500 arrays with pixel values of one denoting the location of the ground-truth γ -ray energies and zeroes in all other bins. The training and target spectra were padded with 12 empty bins on their top and right edges to bring their size to 512×512 , which allows for repeated downsampling through the UNet architecture’s 2×2 pooling layers without numerical rounding issues.

3.2. Train-Test Split and Standardization

We followed standard machine learning methodology in estimating the generalization error of our trained models, by dividing our data into disjoint training and test sets. We used an 80-20 split that yielded a total of 15520 training spectra and 3881 testing spectra. The train and test sets were also standardized to have a mean of zero and unit variance to account for the differences in detection efficiency across SuN’s energy range. Example post-standardization training spectra and their corresponding labels are shown in Figure 2.

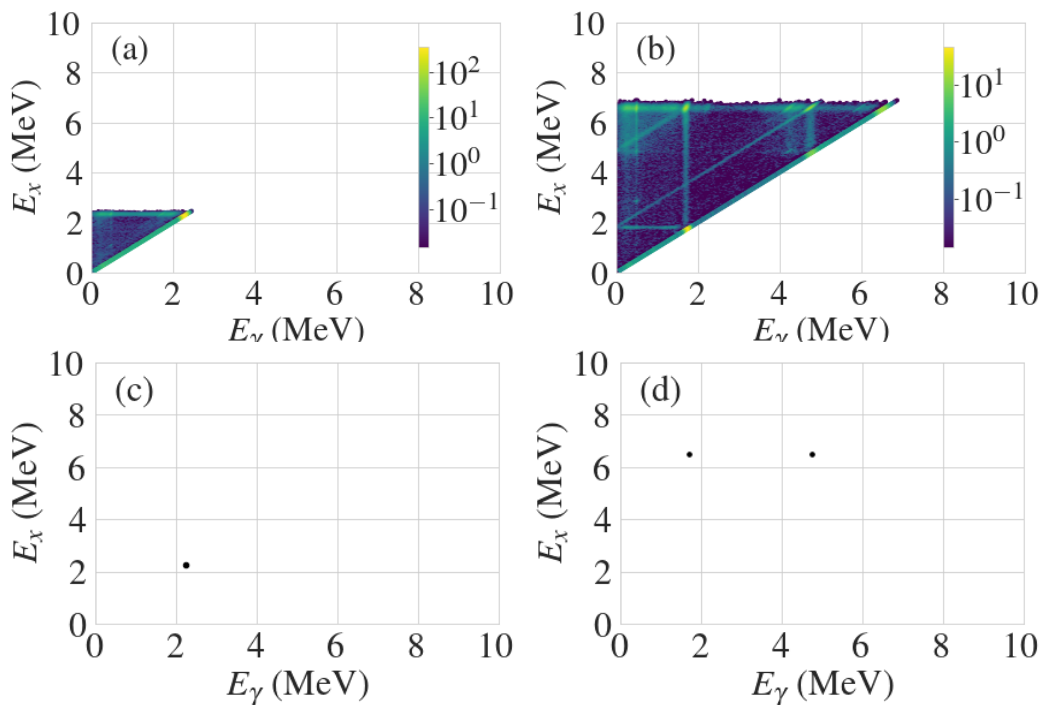


Figure 2: Example training spectra and targets. Subfigures (a) and (b) respectively show single- γ and double- γ (E_x, E_γ) matrices from the standardized training set. Subfigures (c) and (d) show the the corresponding (E'_x, E'_γ) matrices to (a) and (b).

4. Evaluation and Results

4.1. Evaluation Methodology

To evaluate the quality of our machine learning-based unfolding procedure, we need a method to compare the spectra output by our model to the

target spectra. This task is complicated by several factors. Firstly, the target spectra are sparse — a 512×512 target matrix only contains one or two non-zero entries, whereas the model output is noisy and thus, dense. This means that standard distance metrics, like computing the L_1 or L_2 norm between the predicted and target spectra, are ill-suited to this task as they yield artificially large errors. They also conflate different sources of error — for example, a prediction that places a single γ -ray prediction one bin away from the correct location could be deemed just as bad as one that places the prediction several MeV away, or one that smears out its predictions over a larger region of energy-space. A different option might be to use \mathcal{L}_G as our performance metric. This choice has the advantage that it measures the quantity that our generator is directly optimizing. However, this metric suffers from the drawback that its value is not directly interpretable from a physics standpoint. To circumvent these issues, we use a two-step evaluation strategy: we first consolidate the output from the model using a clustering algorithm, before computing the L_2 distance between the predicted and true spectrum. We now describe the details of this procedure.

4.1.1. *k*-means Clustering

The *k*-means clustering problem seeks to group a set of n sample observations $\{\mathbf{x}_1, \mathbf{x}_2, \dots, \mathbf{x}_n\}$ into k disjoint clusters $\{C_1, C_2, \dots, C_k\}$ (where $k \leq n$) in a manner that minimizes the variance among the members of each cluster. Each cluster C_j is described by the mean of the points associated to it, denoted by $\boldsymbol{\mu}_j$. Formally, the aim is to solve the following optimization problem:

$$\arg \min_{\boldsymbol{\mu}_j} \sum_{i=1}^n \sum_{j=1}^k \mathbb{1}[x_i \in C_j] \cdot \|\mathbf{x}_i - \boldsymbol{\mu}_j\|^2$$

While solving this problem optimally is NP-hard, heuristic approaches such as Lloyd’s algorithm [46], which iteratively determines the centroids of the k clusters, are often effective in practice.

4.1.2. Clustering Predicted Spectra

We perform two post-processing steps on a matrix output by our model to enable a meaningful comparison to the target spectrum. First, we filter out noise by rounding down to 0 all matrix entries that are less than 0.2. We then apply *k*-means clustering to the coordinates of the non-zero entries in this filtered matrix, with k set to either 1 or 2 depending on the number of

γ -rays in the true spectrum. We use a weighted variant of Lloyd’s algorithm in performing this clustering, using the entries in the matrix as the weights. This approach treats a matrix entry at location (E_x, E_γ) as a measure of the model’s confidence in (E_x, E_γ) being the location of a γ -ray. We use the implementation of Lloyd’s algorithm provided by the `scikit-learn` Python library [47].

4.1.3. L_2 Percentage Error

The centroid(s) returned by the k -means analysis are treated as the model’s effective prediction and compared to the true γ -ray locations using the L_2 distance. We use this as a basis to calculate a percentage error in the model’s prediction, which allows for direct comparison between the model’s results and SuN’s resolution capabilities [15]. As a Sodium Iodide scintillator, SuN’s resolution is inherently limited, generally to within 5–7% of the energy of the measured γ -ray. The resulting width of SuN’s energy peaks affects both the bin distribution of counts in the input spectra and the accuracy limitations on model predictions and percent error metrics provide a reasonable method for determining if a given γ -ray prediction falls within this limitation.

4.2. Results

Table 1 presents the hyperparameter settings that resulted in the best performing model in our experiments. Code and data to train and evaluate these models, as well as a pre-trained model, are available at [48]. Figure 3 shows percentage error results for model predictions on the test set, broken out into single- γ spectra and double- γ spectra. Over 90% (1800/1990) of predictions for single γ -ray testing spectra fell within 5% of the ground truth energy. For two γ -ray test spectra, almost 93% (3517/3782) of predictions fell within 5% of the ground truth energy.

We also investigated model performance on data sourced from actual experiments. We evaluate the model using (E_x, E_γ) matrices for the decays of common γ -ray sources ^{60}Co and ^{137}Cs placed at the center of the SuN detector. ^{137}Cs emits a single γ -ray at 662 keV, and ^{60}Co predominantly decays via the emission of two sequential γ -rays at 1173 and 1332 keV. These results are shown in Figure 4. The 662 keV γ -ray of the ^{137}Cs decay is predicted within bin accuracy, and the 1173 and 1332 keV γ -rays of the ^{60}Co decay are predicted with respective errors of 3.41% and 3.11%.

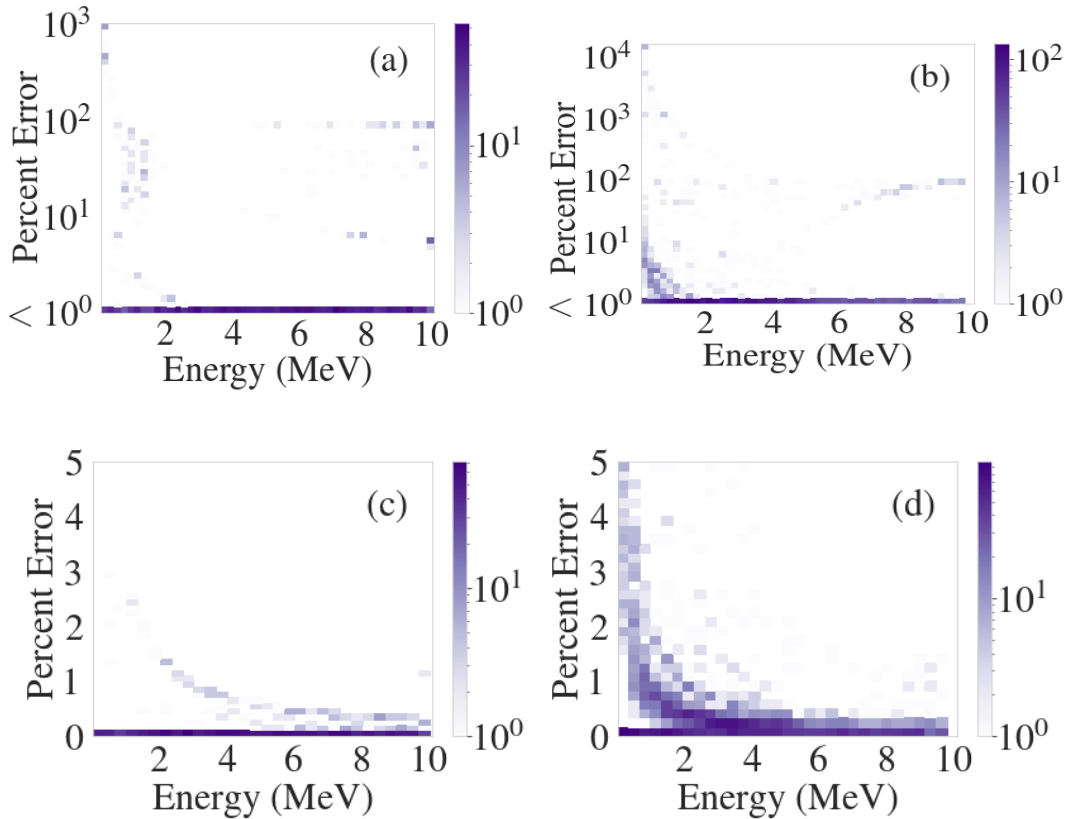


Figure 3: Simulated test set results. Subfigure (a) shows results for single γ -ray test spectra and (b) shows results for test spectra with two γ -ray cascades. Test examples predicted within 5% of the ground truth are shown for single γ -ray spectra in subfigure (c) (90% of test examples) and two γ -ray spectra in (d) (92.9% of total test examples). Color corresponds with frequency of test spectra in a given bin.

5. Conclusions and Future Work

We have demonstrated the effectiveness of conditional GANs in constraining simple nuclear level schemes from (E_x, E_γ) matrices. Our trained cGAN model showed prediction capabilities comparable to the energy resolution of the SuN detector for over 90% of tested single γ -ray spectra and nearly 93% of double γ -ray spectra. Additionally, the model was shown to accurately characterize the level schemes of common sources ^{60}Co and ^{137}Cs from experimentally measured (E_x, E_γ) matrices.

As it stands, this work is a promising proof of concept for the use of

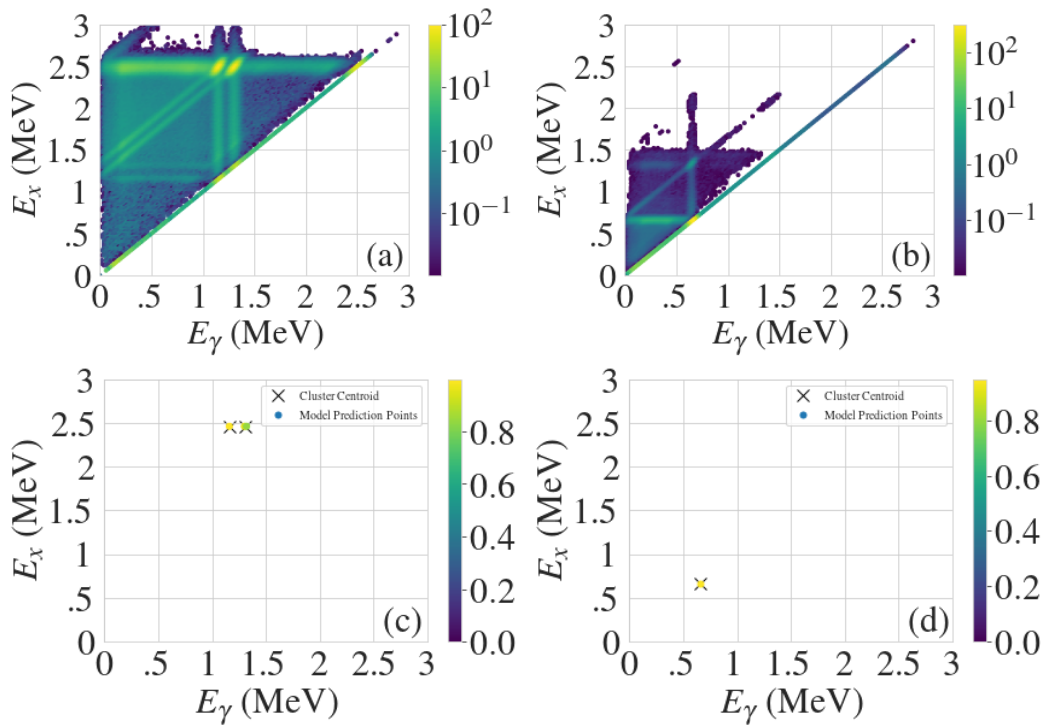


Figure 4: Standardized input and predicted output spectra for experimental data on ^{60}Co and ^{137}Cs decays. Subfigures (a) and (b) show standardized (E_x, E_γ) input matrices for ^{60}Co and ^{137}Cs respectively. Additional counts at energies higher than the true decay result from SuN’s detection of more than one event within a single timing window. Subfigures (c) and (d) show corresponding model predictions with k -means centroids overlaid. Here, all subfigures are zoomed to the first 3MeV for ease of viewing, but the full spectra extend to the same 10MeV limits as the training dataset.

conditional GANs in total absorption spectroscopy analysis and future efforts are planned in several areas. In order to be useful for the analysis of unstable nuclei far from the valley of stability, the model must be trained on increasingly complex decay schemes with more γ -rays of varying intensities. Other improvements to the k -means evaluation process, like the implementation of a convolutional neural network to determine the number of γ -rays present in an output spectrum, will allow for completely automated analysis of unknown level schemes. Taken together, these future plans will expand the model’s applicability, building upon the promise of the work presented here.

6. Acknowledgements

The work was supported by the National Science Foundation under grants PHY 2012865, PHY 1913554, PHY 1430152, PHY 1613188. This work was supported by the US Department of Energy (DOE) National Nuclear Security Administration Grant No DOE-DE-NA0003906 and the DOE Office of Science under Grant No. DE-SC0020451. This material is based upon work supported by the Department of Energy/National Nuclear Security Administration through the Nuclear Science and Security Consortium under Award No. DE-NA0003180.

References

- [1] M. Elyashberg, Identification and structure elucidation by NMR spectroscopy, *TrAC Trends in Analytical Chemistry* 69 (2015) 88–97. URL: <https://www.sciencedirect.com/science/article/pii/S0165993615000874>. doi:<https://doi.org/10.1016/j.trac.2015.02.014>.
- [2] L. Yang, T. Guo, X. Zhang, S. Cao, X. Ding, Toxic chemical compound detection by terahertz spectroscopy: a review, *Reviews in Analytical Chemistry* 37 (2018) 20170021. URL: <https://doi.org/10.1515/revac-2017-0021>. doi:[doi:10.1515/revac-2017-0021](https://doi.org/10.1515/revac-2017-0021).
- [3] J. D. Lowenthal, D. C. Koo, R. Guzman, J. Gallego, A. C. Phillips, S. M. Faber, N. P. Vogt, G. D. Illingworth, C. Gronwall, Keck spectroscopy of redshift $z \sim 3$ galaxies in the Hubble Deep Field, *The Astrophysical Journal* 481 (1997) 673–688. URL: <https://doi.org/10.1086/304092>. doi:[10.1086/304092](https://doi.org/10.1086/304092).
- [4] M. D. Lehnert, N. P. H. Nesvadba, J.-G. Cuby, A. M. Swinbank, S. Morris, B. Clément, C. J. Evans, M. N. Bremer, S. Basa, Spectroscopic confirmation of a galaxy at redshift $z = 8.6$, *Nature* 467 (2010) 940–942. URL: <https://doi.org/10.1038/nature09462>. doi:[10.1038/nature09462](https://doi.org/10.1038/nature09462).
- [5] C. E. Crouthamel, F. Adams, R. Dams, *Applied gamma-ray spectrometry*, volume 41, Elsevier, 2013.

- [6] S. Jhung, S. Hur, G. Cho, I. Kwon, A neural network approach for identification of gamma-ray spectrum obtained from silicon photomultipliers, *Nuclear Instruments and Methods in Physics Research Section A: Accelerators, Spectrometers, Detectors and Associated Equipment* 954 (2020) 161704. URL: <https://www.sciencedirect.com/science/article/pii/S0168900218318163>. doi:<https://doi.org/10.1016/j.nima.2018.12.019>, symposium on Radiation Measurements and Applications XVII.
- [7] S. Galib, P. Bhowmik, A. Avachat, H. Lee, A comparative study of machine learning methods for automated identification of radioisotopes using nai gamma-ray spectra, *Nuclear Engineering and Technology* 53 (2021) 4072–4079. URL: <https://www.sciencedirect.com/science/article/pii/S1738573321003417>. doi:<https://doi.org/10.1016/j.net.2021.06.020>.
- [8] S. Wu, X. Tang, P. Gong, P. Wang, D. Liang, Y. Li, C. Zhou, X. Zhu, Peak-searching method for low count rate γ spectrum under short-time measurement based on a generative adversarial network, *Nuclear Instruments and Methods in Physics Research Section A: Accelerators, Spectrometers, Detectors and Associated Equipment* 1002 (2021) 165262. URL: <https://www.sciencedirect.com/science/article/pii/S0168900221002461>. doi:<https://doi.org/10.1016/j.nima.2021.165262>.
- [9] C. Cobas, Nmr signal processing, prediction, and structure verification with machine learning techniques, *Magnetic Resonance in Chemistry* 58 (2020) 512–519.
- [10] B. Rubio, W. Gelletly, *Beta Decay of Exotic Nuclei*, Springer Berlin Heidelberg, Berlin, Heidelberg, 2009, pp. 99–151. URL: https://doi.org/10.1007/978-3-540-85839-3_4. doi:10.1007/978-3-540-85839-3_4.
- [11] Y. Fujita, B. Rubio, W. Gelletly, Spin–isospin excitations probed by strong, weak and electro-magnetic interactions, *Progress in Particle and Nuclear Physics* 66 (2011) 549–606. URL: <https://www.sciencedirect.com/science/article/pii/S0146641011000573>. doi:<https://doi.org/10.1016/j.ppnp.2011.01.056>.

- [12] J. Hardy, L. Carraz, B. Jonson, P. Hansen, The essential decay of pandemonium: A demonstration of errors in complex beta-decay schemes, *Physics Letters B* 71 (1977) 307–310. URL: <https://www.sciencedirect.com/science/article/pii/0370269377902234>. doi: [https://doi.org/10.1016/0370-2693\(77\)90223-4](https://doi.org/10.1016/0370-2693(77)90223-4).
- [13] J. Tain, A. Algora, J. Agramunt, V. Guadilla, M. Jordan, A. Montaner-Pizá, B. Rubio, E. Valencia, D. Cano-Ott, W. Gelletly, T. Martinez, E. Mendoza, Z. Podolyák, P. Regan, J. Simpson, A. Smith, J. Strachan, A decay total absorption spectrometer for DESPEC at FAIR, *Nuclear Instruments and Methods in Physics Research Section A: Accelerators, Spectrometers, Detectors and Associated Equipment* 803 (2015) 36–46. URL: <https://www.sciencedirect.com/science/article/pii/S016890021501058X>. doi:<https://doi.org/10.1016/j.nima.2015.09.009>.
- [14] M. Karny, K. Rykaczewski, A. Fijałkowska, B. Rasco, M. Wolińska-Cichočka, R. Grzywacz, K. Goetz, D. Miller, E. Zganjar, Modular total absorption spectrometer, *Nuclear Instruments and Methods in Physics Research Section A: Accelerators, Spectrometers, Detectors and Associated Equipment* 836 (2016) 83–90. URL: <https://www.sciencedirect.com/science/article/pii/S0168900216308646>. doi:<https://doi.org/10.1016/j.nima.2016.08.046>.
- [15] A. Simon, S. Quinn, A. Spyrou, A. Battaglia, I. Beskin, A. Best, B. Bucher, M. Couder, P. DeYoung, X. Fang, J. Görres, A. Kontos, Q. Li, S. Liddick, A. Long, S. Lyons, K. Padmanabhan, J. Peace, A. Roberts, D. Robertson, K. Smith, M. Smith, E. Stech, B. Stefanek, W. Tan, X. Tang, M. Wiescher, SuN: Summing NaI(Tl) gamma-ray detector for capture reaction measurements, *Nuclear Instruments and Methods in Physics Research Section A: Accelerators, Spectrometers, Detectors and Associated Equipment* 703 (2013) 16–21. URL: <https://www.sciencedirect.com/science/article/pii/S0168900212013824>. doi:<https://doi.org/10.1016/j.nima.2012.11.045>.
- [16] B. C. Rasco, M. Wolińska Cichočka, A. Fijałkowska, K. P. Rykaczewski, M. Karny, R. K. Grzywacz, K. C. Goetz, C. J. Gross, D. W. Stracener, E. F. Zganjar, J. C. Batchelder, J. C. Blackmon, N. T. Brewer, S. Go, B. Heffron, T. King, J. T. Matta, K. Miernik, C. D. Nesaraja, S. V. Paulauskas, M. M. Rajabali, E. H. Wang, J. A. Winger, Y. Xiao,

- C. J. Zachary, Decays of the three top contributors to the reactor $\bar{\nu}_e$ high-energy spectrum, ^{92}Rb , $^{96\text{gs}}\text{Y}$, and ^{142}Cs , studied with total absorption spectroscopy, *Phys. Rev. Lett.* 117 (2016) 092501. URL: <https://link.aps.org/doi/10.1103/PhysRevLett.117.092501>. doi: 10.1103/PhysRevLett.117.092501.
- [17] B. C. Rasco, K. P. Rykaczewski, A. Fijałkowska, M. Karny, M. Wolińska-Cichocka, R. K. Grzywacz, C. J. Gross, D. W. Stracener, E. F. Zganjar, J. C. Blackmon, N. T. Brewer, K. C. Goetz, J. W. Johnson, C. U. Jost, J. H. Hamilton, K. Miernik, M. Madurga, D. Miller, S. Padgett, S. V. Paulauskas, A. V. Ramayya, E. H. Spejewski, Complete β -decay pattern for the high-priority decay-heat isotopes ^{137}I and ^{137}Xe determined using total absorption spectroscopy, *Phys. Rev. C* 95 (2017) 054328. URL: <https://link.aps.org/doi/10.1103/PhysRevC.95.054328>. doi:10.1103/PhysRevC.95.054328.
- [18] V. Guadilla, A. Algora, J. Tain, J. Agramunt, J. Äystö, J. Briz, D. Cano-Ott, A. Cucoanes, T. Eronen, M. Estienne, M. Fallot, L. Fraile, E. Ganioglu, W. Gelletly, D. Gorelov, J. Hakala, A. Jokinen, D. Jordan, A. Kankainen, V. Kolhinen, J. Koponen, M. Lebois, T. Martinez, M. Monserrate, A. Montaner-Pizá, I. Moore, E. Nácher, S. Origo, H. Penttilä, Z. Podolyak, I. Pohjalainen, A. Porta, P. Regan, J. Reinikainen, M. Reponen, S. Rinta-Antila, B. Rubio, K. Rytönen, T. Shiba, V. Sonnenschein, A. Sonzogni, E. Valencia, V. Vedia, A. Voss, J. Wilson, A.-A. Zakari-Issoufou, First experiment with the NUSTAR/FAIR decay total absorption γ -ray spectrometer (DTAS) at the IGISOL IV facility, *Nuclear Instruments and Methods in Physics Research Section B: Beam Interactions with Materials and Atoms* 376 (2016) 334–337. URL: <https://www.sciencedirect.com/science/article/pii/S0168583X15012628>. doi:<https://doi.org/10.1016/j.nimb.2015.12.018>, proceedings of the XVIIth International Conference on Electromagnetic Isotope Separators and Related Topics (EMIS2015), Grand Rapids, MI, U.S.A., 11-15 May 2015.
- [19] A. Fijałkowska, M. Karny, K. P. Rykaczewski, B. C. Rasco, R. Grzywacz, C. J. Gross, M. Wolińska Cichocka, K. C. Goetz, D. W. Stracener, W. Bielewski, R. Goans, J. H. Hamilton, J. W. Johnson, C. Jost, M. Madurga, K. Miernik, D. Miller, S. W. Padgett, S. V. Paulauskas,

- A. V. Ramayya, E. F. Zganjar, Impact of modular total absorption spectrometer measurements of β decay of fission products on the decay heat and reactor $\bar{\nu}_e$ flux calculation, *Phys. Rev. Lett.* 119 (2017) 052503. URL: <https://link.aps.org/doi/10.1103/PhysRevLett.119.052503>. doi:10.1103/PhysRevLett.119.052503.
- [20] A. Algora, D. Jordan, J. Tain, B. Rubio, J. Agramunt, A. B. Perez-Cerdan, F. Molina, L. Caballero, E. Nácher, A. Krasznahorkay, M. D. Hunyadi, J. Gulyás, A. Vitéz, M. Csatlós, L. Csige, J. Äystö, H. Penttilä, I. D. Moore, T. Eronen, A. Jokinen, A. Nieminen, J. Hakala, P. Karvonen, A. Kankainen, A. Saastamoinen, J. Rissanen, T. Kessler, C. Weber, J. Ronkainen, S. Rahaman, V. Elomaa, S. Rinta-Antila, U. Hager, T. Sonoda, K. Burkard, W. Hüller, L. Batist, W. Gelletly, A. L. Nichols, T. Yoshida, A. A. Sonzogni, K. Peräjärvi, Reactor decay heat in ^{239}Pu : Solving the γ discrepancy in the 4–3000-s cooling period, *Phys. Rev. Lett.* 105 (2010) 202501. URL: <https://link.aps.org/doi/10.1103/PhysRevLett.105.202501>. doi:10.1103/PhysRevLett.105.202501.
- [21] V. Guadilla, A. Algora, J. L. Tain, J. Agramunt, J. Aysto, J. A. Briz, A. Cucoanes, T. Eronen, M. Estienne, M. Fallot, L. M. Fraile, E. Ganioglu, W. Gelletly, D. Gorelov, J. Hakala, A. Jokinen, D. Jordan, A. Kankainen, V. Kolhinen, J. Koponen, M. Lebois, T. Martinez, M. Monserrate, A. Montaner-Piza, I. Moore, E. Nacher, S. E. A. Origo, H. Penttilä, I. Pohjalainen, A. Porta, J. Reinikainen, M. Reponen, S. Rinta-Antila, B. Rubio, K. Rytönen, T. Shiba, V. Sonnenschein, A. A. Sonzogni, E. Valencia, V. Vedia, A. Voss, J. N. Wilson, A. A. Zakari-Issoufou, Study of the β decay of fission products with the dtas detector, *Acta Physica Polonica. Series B* 48 (2017). doi:10.5506/APhysPolB.48.529.
- [22] A. Spyrou, S. N. Liddick, A. C. Larsen, M. Guttormsen, K. Cooper, A. C. Dombos, D. J. Morrissey, F. Naqvi, G. Perdikakis, S. J. Quinn, T. Renstrøm, J. A. Rodriguez, A. Simon, C. S. Sumithrarachchi, R. G. T. Zegers, Novel technique for constraining r -process (n , γ) reaction rates, *Phys. Rev. Lett.* 113 (2014) 232502. URL: <https://link.aps.org/doi/10.1103/PhysRevLett.113.232502>. doi:10.1103/PhysRevLett.113.232502.
- [23] A. Spyrou, A. C. Larsen, S. N. Liddick, F. Naqvi, B. P. Crider, A. C.

- Dombos, M. Guttormsen, D. L. Bleuel, A. Couture, L. C. Campo, R. Lewis, S. Mosby, M. R. Mumpower, G. Perdikakis, C. J. Prokop, S. J. Quinn, T. Renstrøm, S. Siem, R. Surman, Neutron-capture rates for explosive nucleosynthesis: the case of $^{68}\text{Ni}(n,\gamma)^{69}\text{Ni}$, *Journal of Physics G: Nuclear and Particle Physics* 44 (2017) 044002. URL: <https://doi.org/10.1088/1361-6471/aa5ae7>. doi:10.1088/1361-6471/aa5ae7.
- [24] S. N. Liddick, A. Spyrou, B. P. Crider, F. Naqvi, A. C. Larsen, M. Guttormsen, M. Mumpower, R. Surman, G. Perdikakis, D. L. Bleuel, A. Couture, L. Crespo Campo, A. C. Dombos, R. Lewis, S. Mosby, S. Nikas, C. J. Prokop, T. Renstrom, B. Rubio, S. Siem, S. J. Quinn, Experimental neutron capture rate constraint far from stability, *Phys. Rev. Lett.* 116 (2016) 242502. URL: <https://link.aps.org/doi/10.1103/PhysRevLett.116.242502>. doi:10.1103/PhysRevLett.116.242502.
- [25] S. N. Liddick, A. C. Larsen, M. Guttormsen, A. Spyrou, B. P. Crider, F. Naqvi, J. E. Midtbø, F. L. Bello Garrote, D. L. Bleuel, L. Crespo Campo, A. Couture, A. C. Dombos, F. Giacoppo, A. Gørgen, K. Hadynska-Klek, T. W. Hagen, V. W. Ingeberg, B. V. Kheswa, R. Lewis, S. Mosby, G. Perdikakis, C. J. Prokop, S. J. Quinn, T. Renstrøm, S. J. Rose, E. Sahin, S. Siem, G. M. Tveten, M. Wiedeking, F. Zeiser, Benchmarking the extraction of statistical neutron capture cross sections on short-lived nuclei for applications using the β -oslo method, *Phys. Rev. C* 100 (2019) 024624. URL: <https://link.aps.org/doi/10.1103/PhysRevC.100.024624>. doi:10.1103/PhysRevC.100.024624.
- [26] A. Spyrou, H.-W. Becker, A. Lagoyannis, S. Harissopulos, C. Rolfs, Cross-section measurements of capture reactions relevant to the p process using a 4π γ -summing method, *Phys. Rev. C* 76 (2007) 015802. URL: <https://link.aps.org/doi/10.1103/PhysRevC.76.015802>. doi:10.1103/PhysRevC.76.015802.
- [27] C. Reingold, O. Olivas-Gomez, A. Simon, J. Arroyo, M. Chamberlain, J. Wurzer, A. Spyrou, F. Naqvi, A. Dombos, A. Palmisano, T. Anderson, A. Clark, B. Frenzt, M. Hall, S. Henderson, S. Moylan, D. Robertson, M. Skulski, E. Stech, Y. Strauss, W. Tan, B. Vande Kolk, High efficiency total absorption spectrometer HECTOR for capture reaction measurements, *The European Physical*

- Journal A 55 (2019). URL: <https://link.springer.com/article/10.1140/epja/i2019-12748-8#citeas>. doi:<https://doi.org/10.1140/epja/i2019-12748-8>.
- [28] M. Guttormsen, T. Tveter, L. Bergholt, F. Ingebretsen, J. Rekstad, The unfolding of continuum γ -ray spectra, *Nuclear Instruments and Methods in Physics Research Section A: Accelerators, Spectrometers, Detectors and Associated Equipment* 374 (1996) 371–376. URL: <https://www.sciencedirect.com/science/article/pii/0168900296001970>. doi: [https://doi.org/10.1016/0168-9002\(96\)00197-0](https://doi.org/10.1016/0168-9002(96)00197-0).
- [29] R. Koohi-Fayegh, S. Green, N. Crout, G. Taylor, M. Scott, Neural network unfolding of photon and neutron spectra using an ne-213 scintillation detector, *Nuclear Instruments and Methods in Physics Research Section A: Accelerators, Spectrometers, Detectors and Associated Equipment* 329 (1993) 269–276. URL: <https://www.sciencedirect.com/science/article/pii/016890029390946F>. doi: [https://doi.org/10.1016/0168-9002\(93\)90946-F](https://doi.org/10.1016/0168-9002(93)90946-F).
- [30] S. Bailey, T. Kokalova, M. Freer, C. Wheldon, R. Smith, J. Walsh, N. Soić, L. Prpolec, V. Tokić, F. Marqués, L. Achouri, F. Delaunay, M. Parlog, Q. Deshayes, B. Fernández-Dominguez, B. Jacquot, The identification of α -clustered doorway states in $^{44,48,52}\text{Ti}$ using machine learning, *The European Physical Journal A* 57 (2021) 73–79. URL: <https://link.springer.com/article/10.1140/2Fepja%2Fs10050-021-00357-3#citeas>. doi:<https://doi.org/10.1140/epja/s10050-021-00357-3>.
- [31] R. Gladen, V. Chirayath, A. Fairchild, M. Manry, A. Koymen, A. Weiss, Efficient machine learning approach for optimizing the timing resolution of a high purity germanium detector, *Nuclear Instruments and Methods in Physics Research Section A: Accelerators, Spectrometers, Detectors and Associated Equipment* 981 (2020) 164505. URL: <https://www.sciencedirect.com/science/article/pii/S0168900220309025>. doi: <https://doi.org/10.1016/j.nima.2020.164505>.
- [32] M. Kamuda, C. J. Sullivan, An automated isotope identification and quantification algorithm for isotope mixtures in low-resolution gamma-ray spectra, *Radiation Physics and Chemistry* 155 (2019) 281–286. URL: <https://www.sciencedirect.com/science/article/pii/>

S0969806X17308320. doi:<https://doi.org/10.1016/j.radphyschem.2018.06.017>, iRRMA-10.

- [33] M. Kamuda, J. Zhao, K. Huff, A comparison of machine learning methods for automated gamma-ray spectroscopy, *Nuclear Instruments and Methods in Physics Research Section A: Accelerators, Spectrometers, Detectors and Associated Equipment* 954 (2020) 161385. URL: <https://www.sciencedirect.com/science/article/pii/S0168900218313779>. doi:<https://doi.org/10.1016/j.nima.2018.10.063>, symposium on Radiation Measurements and Applications XVII.
- [34] M. Medhat, Artificial intelligence methods applied for quantitative analysis of natural radioactive sources, *Annals of Nuclear Energy* 45 (2012) 73–79. URL: <https://www.sciencedirect.com/science/article/pii/S030645491200059X>. doi:<https://doi.org/10.1016/j.anucene.2012.02.013>.
- [35] E. Fysikopoulos, M. Rouchota, V. Eleftheriadis, C.-A. Gatsiou, I. Pilatis, S. Sarpaki, G. Loudos, S. Kostopoulos, D. Glotsos, Optical to planar x-ray mouse image mapping in preclinical nuclear medicine using conditional adversarial networks, *Journal of Imaging* 7 (2021) 262. URL: <http://dx.doi.org/10.3390/jimaging7120262>. doi:10.3390/jimaging7120262.
- [36] H.-J. Kim, D. Lee, Image denoising with conditional generative adversarial networks (cGAN) in low dose chest images, *Nuclear Instruments and Methods in Physics Research Section A: Accelerators, Spectrometers, Detectors and Associated Equipment* 954 (2020) 161914. URL: <https://www.sciencedirect.com/science/article/pii/S0168900219302293>. doi:<https://doi.org/10.1016/j.nima.2019.02.041>, symposium on Radiation Measurements and Applications XVII.
- [37] F. List, I. Bhat, G. F. Lewis, A black box for dark sector physics: predicting dark matter annihilation feedback with conditional GANs, *Monthly Notices of the Royal Astronomical Society* 490 (2019) 3134–3143. URL: <https://academic.oup.com/mnras/article-pdf/490/3/3134/30327869/stz2759.pdf>. doi:10.1093/mnras/stz2759.
- [38] L. Velasco, E. McClellan, N. Sato, P. Ambrozewicz, T. Liu, W. Melnitchouk, M. Kuchera, Y. Alanazi, Y. Li, cfat-gan: Conditional simula-

- tion of electron–proton scattering events with variate beam energies by a feature augmented and transformed generative adversarial network, in: M. A. Wani, B. Raj, F. Luo, D. Dou (Eds.), *Deep Learning Applications*, Volume 3, Springer Singapore, Singapore, 2022, pp. 245–261. URL: https://doi.org/10.1007/978-981-16-3357-7_10. doi: 10.1007/978-981-16-3357-7_10.
- [39] S. Ahmed, C. Sánchez Muñoz, F. Nori, A. F. Kockum, Quantum state tomography with conditional generative adversarial networks, *Phys. Rev. Lett.* 127 (2021) 140502. URL: <https://link.aps.org/doi/10.1103/PhysRevLett.127.140502>. doi:10.1103/PhysRevLett.127.140502.
- [40] P. Isola, J.-Y. Zhu, T. Zhou, A. A. Efros, Image-to-image translation with conditional adversarial networks, 2018. [arXiv:1611.07004](https://arxiv.org/abs/1611.07004).
- [41] Tensorflow Developers, Pix2pix: Image-to-image translation with a conditional GAN, 2021. <https://www.tensorflow.org/tutorials/generative/pix2pix>.
- [42] O. Ronneberger, P. Fischer, T. Brox, U-net: Convolutional networks for biomedical image segmentation, 2015. [arXiv:1505.04597](https://arxiv.org/abs/1505.04597).
- [43] D. P. Kingma, J. Ba, Adam: A method for stochastic optimization, 2017. [arXiv:1412.6980](https://arxiv.org/abs/1412.6980).
- [44] S. Ruder, An overview of gradient descent optimization algorithms, 2016. URL: <https://arxiv.org/abs/1609.04747>. doi:10.48550/ARXIV.1609.04747.
- [45] S. Agostinelli, J. Allison, K. Amako, J. Apostolakis, H. Araujo, P. Arce, M. Asai, D. Axen, S. Banerjee, G. Barrand, F. Behner, L. Bellagamba, J. Boudreau, L. Broglio, A. Brunengo, H. Burkhardt, S. Chauvie, J. Chuma, R. Chytráček, G. Cooperman, G. Cosmo, P. Degtyarenko, A. Dell’Acqua, G. Depaola, D. Dietrich, R. Enami, A. Feliciello, C. Ferguson, H. Fesefeldt, G. Folger, F. Foppiano, A. Forti, S. Garelli, S. Giani, R. Giannitrapani, D. Gibin, J. Gómez Cadenas, I. González, G. Gracia Abril, G. Greeniaus, W. Greiner, V. Grichine, A. Grossheim, S. Guatelli, P. Gumplinger, R. Hamatsu, K. Hashimoto, H. Hasui, A. Heikkinen, A. Howard, V. Ivanchenko, A. Johnson, F. Jones, J. Kallenbach, N. Kanaya, M. Kawabata, Y. Kawabata, M. Kawaguti, S. Kelner,

- P. Kent, A. Kimura, T. Kodama, R. Kokoulin, M. Kossov, H. Kurashige, E. Lamanna, T. Lampén, V. Lara, V. Lefebure, F. Lei, M. Liendl, W. Lockman, F. Longo, S. Magni, M. Maire, E. Medernach, K. Minamimoto, P. Mora de Freitas, Y. Morita, K. Murakami, M. Nagamatu, R. Nartallo, P. Nieminen, T. Nishimura, K. Ohtsubo, M. Okamura, S. O’Neale, Y. Oohata, K. Paech, J. Perl, A. Pfeiffer, M. Pia, F. Ranjard, A. Rybin, S. Sadilov, E. Di Salvo, G. Santin, T. Sasaki, N. Savvas, Y. Sawada, S. Scherer, S. Sei, V. Sirotenko, D. Smith, N. Starkov, H. Stoecker, J. Sulkimo, M. Takahata, S. Tanaka, E. Tcherniaev, E. Safai Tehrani, M. Tropeano, P. Truscott, H. Uno, L. Urban, P. Urban, M. Verderi, A. Walkden, W. Wander, H. Weber, J. Wellisch, T. Wenaus, D. Williams, D. Wright, T. Yamada, H. Yoshida, D. Zschesche, Geant4—a simulation toolkit, *Nuclear Instruments and Methods in Physics Research Section A: Accelerators, Spectrometers, Detectors and Associated Equipment* 506 (2003) 250–303. URL: <https://www.sciencedirect.com/science/article/pii/S0168900203013688>. doi: [https://doi.org/10.1016/S0168-9002\(03\)01368-8](https://doi.org/10.1016/S0168-9002(03)01368-8).
- [46] S. Lloyd, Least squares quantization in pcm, *IEEE Transactions on Information Theory* 28 (1982) 129–137. doi:10.1109/TIT.1982.1056489.
- [47] F. Pedregosa, G. Varoquaux, A. Gramfort, V. Michel, B. Thirion, O. Grisel, M. Blondel, P. Prettenhofer, R. Weiss, V. Dubourg, J. Vanderplas, A. Passos, D. Cournapeau, M. Brucher, M. Perrot, E. Duchesnay, Scikit-learn: Machine learning in Python, *Journal of Machine Learning Research* 12 (2011) 2825–2830.
- [48] C. Dembski, SuN_cGAN, 2022. URL: https://github.com/alpha-davidson/SuN_cGAN/releases/tag/v1.0. doi: 10.5821/zenodo.6703859.